Supplementary Information for "Quantum nondemolition measurement of mechanical squeezed state beyond the 3 dB limit"

C. U. Lei,[1] A. J. Weinstein,[1] J. Suh,[2] E. E. Wollman,[1] A. Kronwald,[3,4] F. Marquardt,[3,4] A. A. Clerk,[5] K. C. Schwab[1]
[1] *Applied Physics, California Institute of Technology, Pasadena, CA 91125, USA*
[2] *Korea Research Institute of Standards and Science, Daejeon 305-340, Republic of Korea*
[3] *Friedrich-Alexander-Universität Erlangen-Nürnberg, Staudtstr. 7, D-91058 Erlangen, Germany*
[4] *Max Planck Institute for the Science of Light Günther-Scharowsky-Straße 1/Bau 24, D-91058 Erlangen, Germany and*
[5] *Department of Physics, McGill University, Montreal, Quebec, H3A 2T8 Canada*
(Dated: July 26, 2016)

I. THEORY

A. Ideal two tones optomechanical Hamiltonian

The Hamiltonian of a generic optomechanical system reads

$$\hat{H} = \hbar\omega_c \hat{a}^\dagger \hat{a} + \hbar\omega_m \hat{b}^\dagger \hat{b} - \hbar g_0 \hat{a}^\dagger \hat{a} \left(\hat{b} + \hat{b}^\dagger\right) + \hat{H}_{\rm drive}, \tag{1}$$

where $\hat{a}$ $\left(\hat{a}^\dagger\right)$ is the annihilation (creation) operator of the intra-cavity field, $\hat{b}$ $\left(\hat{b}^\dagger\right)$ is the mechanical phonon annihilation (creation) operator, and g_0 is the bare optomechanical coupling between the cavity and the mechanical oscillator. $\hat{H}_{\rm drive}$ describes the external driving.

The device studied in this work is a two ports optomechanical system. Microwave tones are applied from the left port, which we designate (L). In this section, we consider a system driven by two microwave tones. The drive Hamiltonian reads

$$\hat{H}_{\rm drive} = \hbar\sqrt{\kappa_{\rm L}} \sum_{\nu=\pm} \alpha_\nu \left(\hat{a} e^{i\omega_\nu t} + \hat{a}^\dagger e^{-i\omega_\nu t}\right), \tag{2}$$

where $\omega_\pm = \omega_c + \Delta \pm (\omega_m + \delta)$ and $\alpha_\pm$ are the blue and red pump amplitudes at the input port. In the following, we apply the standard linearization – i.e., we separate the cavity and the mechanical operators, $\hat{a}$ and $\hat{b}$, into a classical part, $\bar{a}$ or $\bar{b}$, plus quantum fluctuations, $\hat{d}$ or $\hat{b}$. E.g., $\hat{a} \to \bar{a} + \hat{d}$. In the interaction picture with respect to $\hat{H}_0 = \hbar\left(\omega_c + \Delta\right)\hat{a}^\dagger \hat{a} + \hbar\left(\omega_m + \delta\right)\hat{b}^\dagger \hat{b}$, we find the *linearized* optomechanical Hamiltonian

$$\hat{H} = \hat{H}_{\rm RWA} + \hat{H}_{\rm CR}\,. \tag{3}$$

Here,

$$\hat{H}_{\rm RWA} = -\hbar\Delta \hat{d}^\dagger \hat{d} - \hbar\delta \hat{b}^\dagger \hat{b} - \hbar\left[\left(G_+ \hat{b}^\dagger + G_- \hat{b}\right)\hat{d}^\dagger + \left(G_+ \hat{b} + G_- \hat{b}^\dagger\right)\hat{d}\right] \tag{4}$$

describes the resonant part of the linearized optomechanical interaction whereas

$$\hat{H}_{\rm CR} = -\hbar\left[G_+ e^{-2i(\omega_m+\delta)t}\hat{b} + G_- e^{2i(\omega_m+\delta)t}\hat{b}^\dagger\right]\hat{d}^\dagger - \hbar\left[G_+ e^{2i(\omega_m+\delta)t}\hat{b}^\dagger + G_- e^{-2i(\omega_m+\delta)t}\hat{b}\right]\hat{d} \tag{5}$$

describes off-resonant optomechanical interactions. Note that $G_\pm = g_0 \bar{a}_\pm$ describes the driven-enhanced optomechanical coupling. Here, $\bar{a}_\pm$ is the intracavity microwave amplitude due to the red and blue pumps, and we have assumed $\bar{a}_\pm \in \mathbb{R}$ for simplicity and without loss of generality. In the following analysis, we consider the good cavity limit ($\omega_m \gg \kappa$). At this limit, the off-resonant part of the Hamiltonian can be neglected by the rotating wave approximation (RWA).

B. Mechanical parametric modulation

In addition to the ideal optomechanical interaction, mechanical parametric modulation is observed in the experiment. This spurious mechanical parametric effect can be induced by thermal effects or nonlinearities [1, 2]. To take this effect into account, we phenomenologically include the mechanical parametric interaction

$$\hat{H}_{\rm para} = -\hbar\lambda(e^{i\psi}\hat{b}^2 + e^{-i\psi}\hat{b}^{\dagger 2}), \tag{6}$$

where λ is the amplitude of the parametric interaction, ψ is the relative phase between the parametric drive and the squeezing pump.

C. Quantum Langevin equations

The linearized quantum Langevin equations read

$$\dot{\hat{d}} = -\left(\frac{\kappa}{2} - i\Delta\right)\hat{d} + i\left(G_-\hat{b} + G_+\hat{b}^\dagger\right) + \sqrt{\kappa}\hat{d}_{\rm in}, \tag{7}$$

$$\dot{\hat{b}} = -\left(\frac{\Gamma_m}{2} - i\delta\right)\hat{b} - i2\lambda e^{-i\psi}\hat{b}^\dagger + i\left(G_-\hat{d} + G_+\hat{d}^\dagger\right) + \sqrt{\Gamma_m}\hat{b}_{\rm in}\,. \tag{8}$$

Here, $\hat{d}_{\rm in} = \sum_{\sigma=L,R,I}\sqrt{\frac{\kappa_\sigma}{\kappa}}\hat{d}_{\sigma,\rm in}$ is the total input noise of the cavity, where $\hat{d}_{\sigma,\rm in}$ describes the input fluctuations to the cavity from channel σ with damping rate κ_σ. $\sigma = L$ and R correspond to the left and right microwave cavity ports, while $\sigma = I$ corresponds to internal losses. The noise operator $\hat{c}_{\rm in}$ describes quantum and thermal noise of the mechanical oscillator with intrinsic damping rate Γ_m. The input field operators satisfy the following commutation relations:

$$\left[\hat{d}_{\sigma,\rm in}(t), \hat{d}^\dagger_{\sigma',\rm in}(t')\right] = \delta_{\sigma,\sigma'}\delta(t-t'), \tag{9}$$

$$\left[\hat{b}_{\rm in}(t), \hat{b}^\dagger_{\rm in}(t')\right] = \delta(t-t'), \tag{10}$$

$$\left\langle \hat{d}^\dagger_{\sigma',\rm in}(t)\,\hat{d}_{\sigma,\rm in}(t')\right\rangle = n^{\rm th}_\sigma\delta_{\sigma,\sigma'}\delta(t-t'), \tag{11}$$

$$\left\langle \hat{b}^\dagger_{\rm in}(t)\,\hat{b}_{\rm in}(t')\right\rangle = n^{\rm th}_m\delta(t-t'), \tag{12}$$

where $n^{\rm th}_\sigma$ is the photon occupation in port σ, and $n^{\rm th}_m = 1/\left[\exp\left(\hbar\omega_m/k_BT\right) - 1\right]$ is the thermal occupation of the mechanical oscillator. The total occupation of the cavity is the weighted sum of the contributions from different channels: $n^{\rm th}_c = \sum_\sigma \frac{\kappa_\sigma}{\kappa} n^{\rm th}_\sigma$.

D. Optomechanical output spectrum and mechanical spectrum

In this section, we derive the optomechanical output spectrum and the mechanical quadrature spectrum. For this, we solve the quantum Langevin equations (Eqs. 7, 8) in Fourier space. It is convenient to define the vectors $\boldsymbol{D} = \left(\hat{d}, \hat{d}^\dagger, \hat{b}, \hat{b}^\dagger\right)^T$, $\boldsymbol{D}_{\rm in} = \left(\hat{d}_{\rm in}, \hat{d}^\dagger_{\rm in}, \hat{b}_{\rm in}, \hat{b}^\dagger_{\rm in}\right)^T$ and $\boldsymbol{L} = \mathrm{diag}\left(\sqrt{\kappa}, \sqrt{\kappa}, \sqrt{\Gamma_m}, \sqrt{\Gamma_m}\right)$. We then find the following solution to the quantum Langevin equations in frequency space:

$$\hat{\boldsymbol{D}}[\omega] = \boldsymbol{\chi}[\omega]\cdot\boldsymbol{L}\cdot\hat{\boldsymbol{D}}_{\rm in}[\omega], \tag{13}$$

where

$$\boldsymbol{\chi}[\omega] \equiv \begin{pmatrix} \frac{\kappa}{2} - i(\omega+\Delta) & 0 & -iG_- & -iG_+ \\ 0 & \frac{\kappa}{2} - i(\omega-\Delta) & iG_+ & iG_- \\ -iG_- & -iG_+ & \frac{\Gamma_m}{2} - i(\omega+\delta) & i2\lambda e^{-i\psi} \\ iG_+ & iG_- & -i2\lambda e^{i\psi} & \frac{\Gamma_m}{2} - i(\omega-\delta) \end{pmatrix}^{-1}. \tag{14}$$

In the experiment, we measure the output microwave spectrum through the undriven (right) cavity port. One finds the output field $\hat{d}_{R,\rm out}(\omega)$ using the input-output relation $\hat{d}_{\sigma,\rm out}(\omega) = \hat{d}_{\sigma,\rm in}(\omega) - \sqrt{\kappa_\sigma}\hat{d}(\omega)$. This yields

$$\hat{d}_{R,\rm out}(\omega) = \hat{d}_{R,\rm in}(\omega) - \sqrt{\kappa_R\kappa}\left(\boldsymbol{\chi}[\omega]\right)_{11}\hat{d}_{\rm in} - \sqrt{\kappa_R\kappa}\left(\boldsymbol{\chi}[\omega]\right)_{12}\hat{d}^\dagger_{\rm in} - \sqrt{\kappa_R\Gamma_m}\left(\boldsymbol{\chi}[\omega]\right)_{13}\hat{b}_{\rm in} - \sqrt{\kappa_R\Gamma_m}\left(\boldsymbol{\chi}[\omega]\right)_{14}\hat{b}^\dagger_{\rm in}. \tag{15}$$

The transmission spectrum (driven response) is

$$S_{21}[\omega] = -\sqrt{\kappa_L\kappa_R}\left(\boldsymbol{\chi}[\omega]\right)_{11}. \tag{16}$$

The symmetric noise spectral density is

$$\bar{S}_R[\omega] = \frac{1}{2}\int dt\left\langle\left\{\hat{d}^\dagger_{R,\rm out}[0], \hat{d}_{R,\rm out}[t]\right\}\right\rangle e^{i\omega t} = \frac{1}{2} + \kappa_R S[\omega], \tag{17}$$

where

$$S[\omega] = \kappa\left|\left(\boldsymbol{\chi}[\omega]\right)_{11}\right|^2 n^{\rm th}_{\rm c} + \kappa\left|\left(\boldsymbol{\chi}[\omega]\right)_{12}\right|^2\left(n^{\rm th}_c + 1\right) + \Gamma_m\left|\left(\boldsymbol{\chi}[\omega]\right)_{13}\right|^2 n^{\rm th}_m + \Gamma_m\left|\left(\boldsymbol{\chi}[\omega]\right)_{14}\right|^2\left(n^{\rm th}_m + 1\right). \tag{18}$$

The mechanical quadrature spectrum is

$$\bar{S}_{X_\phi}[\omega] = \frac{1}{2}\int dt \left\langle \left\{ \hat{X}_\phi(t), \hat{X}_\phi(0) \right\} \right\rangle e^{i\omega t}, \tag{19}$$

where $\hat{X}_\phi = x_{\rm zp}\left(\hat{b}e^{i\phi} + \hat{b}^\dagger e^{-i\phi}\right)$. The quadrature variance is given by the integral

$$\left\langle \hat{X}_\phi^2 \right\rangle = \int \frac{d\omega}{2\pi} \bar{S}_{X_\phi}(\omega). \tag{20}$$

In some pump configurations, we can simplify the results. For $\delta = 0$, the expressions can be simplified to

$$S_{21}[\omega] = -\frac{2\sqrt{\kappa_L \kappa_R}\left(\Gamma_m - 2i\omega\right)}{4G^2 + \left[\kappa - 2i\left(\omega + \Delta\right)\right]\left(\Gamma_m - 2i\omega\right)}, \tag{21}$$

$$S[\omega] = \frac{4\Gamma_m\left[\Gamma_m \kappa n_{\rm c}^{\rm th} + 4G_-^2 n_m^{\rm th} + 4G_+^2\left(n_m^{th}+1\right)\right] + 16\kappa n_{\rm c}^{\rm th}\omega^2}{\left|4G^2 + \left(\kappa + 2i\omega\right)\left[\Gamma_m + 2i\left(\omega+\Delta\right)\right]\right|^2}, \tag{22}$$

where $G^2 = G_-^2 - G_+^2$. For both $\delta = 0$ and $\Delta = 0$, the mechanical quadrature spectra and the quadrature variances are

$$\bar{S}_{X_{1,2}}[\omega] = 4x_{zp}^2 \frac{4\kappa\left(G_- \mp G_+\right)^2\left(n_{\rm c}^{\rm th} + \frac{1}{2}\right) + \Gamma_m\left(\kappa^2 + 4\omega^2\right)\left(n_m^{\rm th} + \frac{1}{2}\right)}{\left[4G^2 + \Gamma_m\kappa\right]^2 + 4\left(\Gamma_m^2 + \kappa^2 - 8G^2\right)\omega^2 + 16\omega^4}. \tag{23}$$

$$\left\langle \hat{X}_{1,2}^2 \right\rangle = x_{zp}^2 \frac{4\left(G_- \mp G_+\right)^2\kappa\left(2n_{\rm c}^{\rm th}+1\right) + \left[4G^2 + \kappa\left(\kappa + \Gamma_m\right)\right]\Gamma_m\left(2n_m^{\rm th}+1\right)}{\left(\kappa + \Gamma_m\right)\left(4G^2 + \kappa\Gamma_m\right)}, \tag{24}$$

in the regime $\kappa \gg G, \Gamma_m$, Eq. (24) reduced to Eq. (4) in the main text.

II. MEASUREMENT CIRCUIT

The schematic of the measurement circuit is shown in Fig. S1 We cool the device down to 10 mK with a dilution refrigerator. In the experiment, up to four microwave drives are applied to the device. Because the excess phase noise from the microwave sources at the cavity resonance can excite the cavity and degrade the squeezing, a tunable notch filter cavity is used to provide more than 50 dB noise rejection at the cavity resonance frequency ω_c. The input microwave pumps are then attenuated by about 40 dB at different temperature stages in the cryostat to dissipate the Johnson noise from higher temperature, keeping the input microwave noise at the shot noise level. The output signal passes through two cryocirculators at 50mK, then amplified by a cryogenic high electron-mobility transistor amplifier (HEMT) at 4.2 K and a low noise amplifier at room temperature for analysis. During the measurement of the noise spectrum, we continuously monitor the phase difference between the squeezing pumps and the BAE probes. The beat tones of the pumps and the probes are acquired by microwave detection diodes, then fed into the sub-harmonic circuits to halve the frequencies. The relative phase between the resulting beat tones are compared and measured by the lock-in. A computer is used to generate the error signal and feedback to the sources to keep the phase drift within half degrees.

III. CALIBRATIONS

A. Calibrations of the squeezing output spectrum

In the experiment, we spend an equal time interleaving measurement to measure the pumped noise spectrum $\bar{S}_{\rm meas}[\omega]$ and the unpumped noise spectrum $\bar{S}_0[\omega]$ at the output of the measurement chain. The unpumped noise spectrum $\bar{S}_0[\omega]$ is the noise floor of the system which is dominated by the noise figure of the cryogenic HEMT amplifier. The difference of the pumped and unpumped noise spectra is related to the output noise spectrum of the optomechanical system by

$$\Delta\bar{S}_{\rm meas}[\omega] = \bar{S}_{\rm meas}[\omega] - \bar{S}_0[\omega] = \mathcal{G}[\omega_c]\,\kappa_R\hbar\omega_c S\left[G_-, G_+, \Delta, \delta, \kappa, \Gamma_m, n_c^{th}, n_m^{th}, \omega\right], \tag{25}$$

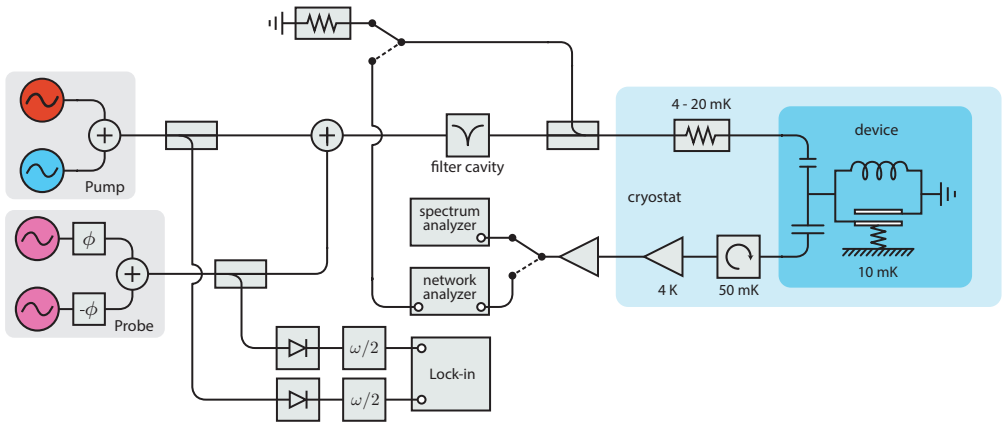

FIG. S1. Schematic of the measurement circuit. See text for detail.

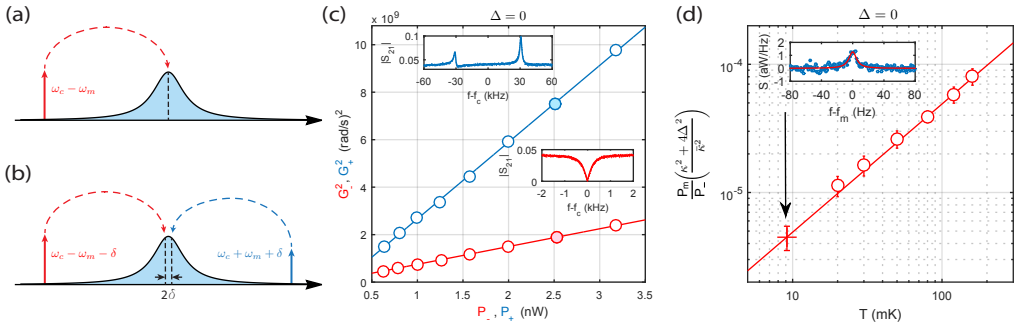

FIG. S2. Calibrations of the mechanical squeezing experiment. (a) Pump configuration of the enhanced optomechanical coupling (G_-) calibration. (b) Pump configuration of the enhanced optomechanical coupling (G_+) calibration. (c) Calibrations of the enhanced optomechanical couplings $G_\pm$, the inserts are the transmission spectrums corresponding to the solid circles. (d) Calibration of the normalized motional sideband power, the insert is the sideband spectrum at the base temperature.

where $\mathcal{G}[\omega]$ is the gain of the measurement chain which is flat in the measurement bandwidth of the experiment and κ_R is the coupling rate to the output port of the device. In order to fit the measured noise spectrum with the optomechanical model (Eq. (18)), an independent measurement of the prefactor $\mathcal{G}[\omega_c]\kappa_R\hbar\omega_c$ is required. Which can be obtained from the calibrations of the enhanced optomechanical couplings and the thermal calibration.

1. *Calibrations of the enhanced optomechanical couplings*

To calibrate the enhanced optomechanical couplings $G_\pm$, we measure the transmitted power of the drive tones at the output of the measurement chain $P_\pm$, which is related to the intracavity pump photon number by

$$P_\pm = \mathcal{G}[\omega_\pm]\kappa_R\hbar\omega_\pm\lambda[\omega_\pm]n_p^\pm, \tag{26}$$

where $\lambda[\omega_\pm]$ are the correction factors due to the parasitic channel [3]. The square of the enhanced optomechanical couplings are related linearly to the transmitted pump powers by

$$G_\pm^2 = g_0^2 n_p^\pm = a_\pm \times P_\pm, \tag{27}$$

where the $a_\pm = \frac{1}{\mathcal{G}[\omega_\pm]\kappa_R\hbar\omega_\pm}\frac{g_0^2}{\lambda[\omega_\pm]}$ is the calibrations of the enhanced optomechanical couplings.

We start with the calibration of the enhanced optomechanical coupling G_- induced by the red detuned tone. To do that, a single red detuned tone is applied at $\omega_c - \omega_m$ with transmitted power P_- (Fig. S2a). Then, a network analyzer is used to generate a weak probe and sweep it through the center of the cavity resonance to measure the transmission spectrum of the mechanical sideband. The enhanced optomechanical coupling rate G_- can be extracted by fitting the transmission spectrum with the optomechanical model (16). By measuring the transmission spectrum

with various transmitted power P_- and fitting with the linear relation (27) (the red line in Fig. S2c), we obtain the calibration $a_- = (7.49 \pm 0.10) \times 10^{17}\,\mathrm{rad^2 s^{-1} W^{-1}}$ and the intrinsic mechanical linewidth $\Gamma_m = 2\pi \times 8$ Hz.

A similar method is used to calibrate the enhanced optomechanical coupling G_+ induced by the blue detuned tone. In this case, a blue detuned tone is placed at $\omega_c + \omega_m + \delta$ with transmitted power P_+ and $\delta = 2\pi \times 30\mathrm{kHz} \ll \kappa$. Because the blue detuned tone would amplify the mechanical motion and narrow the mechanical linewidth, the mechanical resonator becomes unstable when the cooperativity $C_+ = \frac{4G_+^2}{\kappa\Gamma_m}$ approaches to unity. In order to keep the mechanics stable, a constant red detuned tone is applied at $\omega_c - \omega_m - \delta$ to damp the mechanical motion (Fig. S2b). Similar to the calibration of G_-, we measure the transmission spectrum of the mechanical sidebands with the spectrum analyzer and extract the enhanced optomechanical coupling rate G_+ from the fit at various transmitted power P_+. The linear fit (blue line in Fig. S2c) gives $a_+ = (3.23 \pm 0.07) \times 10^{18}\,\mathrm{rad^2 s^{-1} W^{-1}}$.

2. Thermal calibration

Having calibrated the enhanced optomechanical couplings, we turn to the thermal calibration of the motional sideband noise power. To do that, a single red detuned tone is placed at $\omega_- = \omega_c - \omega_m$ with sufficiently small pump power P_- such that the optomechanical damping effect is negligible ($\Gamma_{\mathrm{opt}}^- = \frac{4G_-^2}{\kappa} \ll \Gamma_m$). We then measure the noise power of the up-converted motional sideband P_m^- over a range of calibrated cryostat temperature T (Fig. S2d). Due to the weak temperature dependence of the cavity linewidth κ, we monitor the cavity linewidth at each measurement temperature. The resulting normalized sideband power is given by

$$\left(\frac{4\Delta^2 + \kappa^2}{\bar{\kappa}^2}\right)\frac{P_m}{P_-} = b_- \left(\frac{2}{\bar{\kappa}}\right)^2 \frac{k_B T}{\hbar\omega_m}, \tag{28}$$

where $\Delta = \omega_- - \omega_c + \omega_m$ which is equal to zero in this case, $\bar{\kappa}$ is the average value of the cavity linewidth over the respective temperatures and $b_- = \frac{\mathcal{G}[\omega_c]\omega_c}{\mathcal{G}[\omega_-]\omega_-}\frac{g_0^2}{\lambda[\omega_-]}$ is the thermal calibration. The linear fit in Fig. S2d gives $b_- = (2.53 \pm 0.07) \times 10^5\ (\mathrm{rad/s})^2$, which enables us to convert the normalized noise power into quanta. The prefactor $\mathcal{G}[\omega_c]\kappa_R\hbar\omega_c$ is given by the ratio of the thermal calibration b_- and the calibration of the enhanced optomechanical coupling a_- (i.e. $\mathcal{G}[\omega_c]\kappa_R\hbar\omega_c = b_-/a_-$), which allow us to relate the measured noise spectrum to the optomechanical model

$$\Delta\bar{S}_{\mathrm{meas}}[\omega] = \frac{b_-}{a_-}\bar{S}\left[G_-, G_+, \Delta, \delta, \kappa, \Gamma_m, n_c^{\mathrm{th}}, n_m^{\mathrm{th}}, \omega\right]. \tag{29}$$

3. Fitting procedure

In order to extract the cavity occupation n_c^{th} and the phonon bath occupation n_m^{th} from the output spectrum. We need to determine the enhanced optomechanical couplings $G_\pm$, the detunings Δ and δ, the cavity linewidth κ and the intrinsic mechanical linewidth Γ_m. To obtain these parameters, we measure the transmitted pump power of the microwave drives at each pump configuration, from which we obtain the enhanced optomechanical couplings $G_\pm$ with the calibrations $a_\pm$. Since the resonance frequencies of the cavity and the mechanical mode change with the powers of the microwave drives due to thermal effects [2] and nonlinearties [1], to precisely align the frequencies of the drive tones at $\omega_c \pm \omega_m$, we measure the transmission spectrum to extract the detunings and correct the frequencies of the drives. Fig. S3 shows examples of the measured driven responses (dots) and the corresponding fits (solid curves) at various pump photon ratios. By fitting the transmission spectrum with Eq. (16), we can extract the detunings (δ, Δ) and the cavity linewidth κ, which enable us to correct the frequencies of the drive tones. By iterating this procedures, we can precisely set the powers and the frequencies of the microwave drives. Together with the intrinsic mechanical linewidth Γ_m obtained from the calibration, we can fit the output noise spectrum with the optomechanical model and extract the occupation factors (n_c^{th}, n_m^{th}) with Eq. (29). Fig. S4 shows examples of the noise spectra and the corresponding fits.

B. Calibrations of the backaction evasion spectrum

In our experiment, we perform an additional BAE measurement away from the cavity resonance to directly and independently measure the mechanical quadratures. Since the detuning of the BAE sideband $\Delta = 2\pi \times 160\mathrm{kHz}$

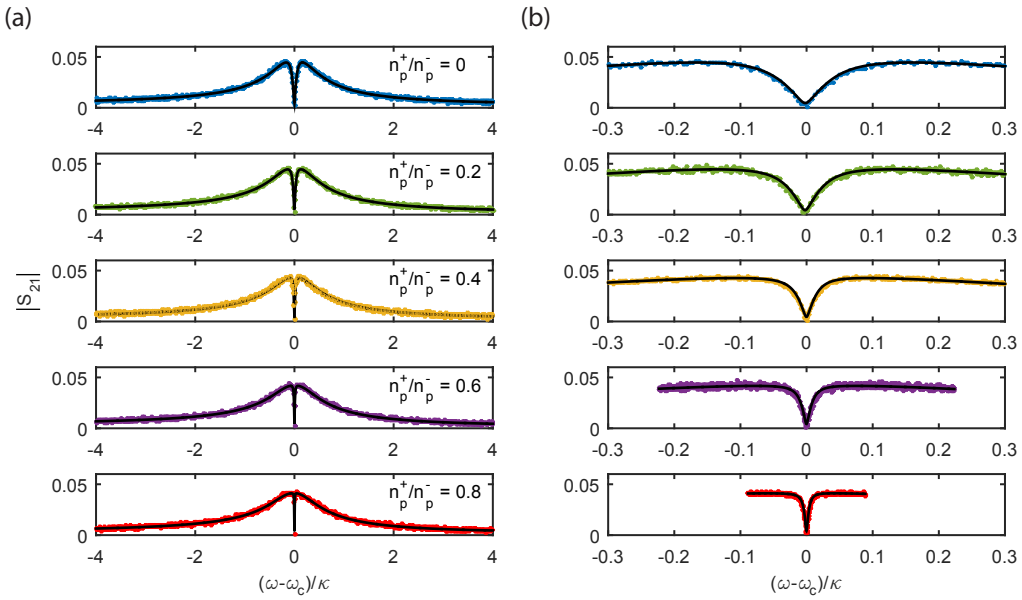

FIG. S3. Amplitude of the transmission spectra at $n_p^{\rm tot} = 1.85 \times 10^5$ and pump photon ratio $n_p^+/n_p^- = 0$ (blue), 0.2 (green), 0.4 (yellow), 0.6 (purple), 0.8 (red). The black curves are the corresponding fits with Eq. (16) (a) Amplitude of the transmission spectra in cavity span. (b) Amplitude of the transmission spectra near the cavity resonance.

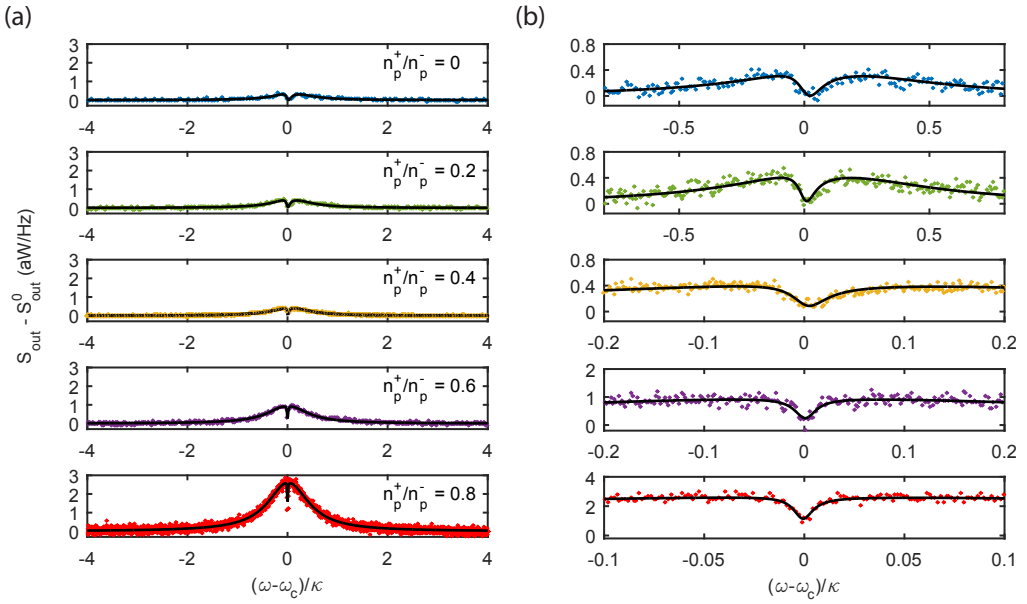

FIG. S4. Output noise spectra at $n_p^{\rm tot} = 1.85 \times 10^5$ and pump photon ratio $n_p^+/n_p^- = 0$ (blue), 0.2 (green), 0.4 (yellow), 0.6 (purple), 0.8 (red). The black curves are the corresponding fits with Eq. (29) and (18) (a) Output noise spectra in cavity span. (b) Output noise spectra near the cavity resonance.

is comparable to the cavity linewidth, to precisely balance the BAE tones and correctly interpret the BAE noise spectrum, an independent calibrations of the enhanced optomechanical coupling rate $G_\pm$ and the normalized sideband power are necessary.

We follow the same procedures in the last section to calibrate the BAE measurement, the only difference is the frequency of the drive tones. Fig. S5a and S5b are the pump configurations in the calibrations of the enhanced optomechanical couplings G_- and G_+. The results of the calibrations are shown in Fig. S5c. From the linear

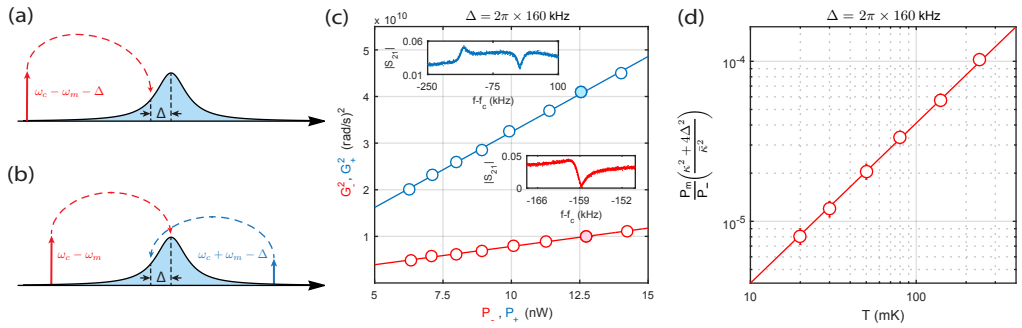

FIG. S5. Calibrations of the backaction evading measurement. (a) Pump configuration of the enhanced optomechanical coupling (G_-) calibration. (b) Pump configuration of the enhanced optomechanical coupling (G_+) calibration. (c) Calibrations of the enhanced optomechanical couplings $G_\pm$, the inserts are the transmission spectrums corresponding to the solid circles. (d) Calibration of the normalized motional sideband power.

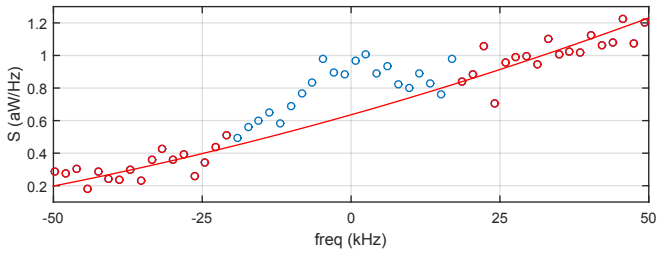

FIG. S6. Example of the BAE noise spectrum. The red line is a background fit with a quadratic polynomial.

fits, we get $a_-^{\mathrm{BAE}} = (7.85 \pm 0.06) \times 10^{17}\,\mathrm{rad^2 s^{-1} W^{-1}}$ and $a_+^{\mathrm{BAE}} = (3.24 \pm 0.03) \times 10^{18}\,\mathrm{rad^2 s^{-1} W^{-1}}$. Fig. S5d is the thermal calibration of the normalized motional sideband power. The linear fit (red line in Fig. S5d) gives $b_-^{\mathrm{BAE}} = (2.77 \pm 0.04) \times 10^5\ (\mathrm{rad/s})^2$.

Similar to the measurement of the squeezing output spectrum, we spend an equal time interleaving measurement to measure the pumped and unpumped noise spectrum. After subtracting the unpumped noise spectrum to remove the noise floor, the output noise spectrum of the BAE measurement is given by

$$\Delta \bar{S}_{\mathrm{meas}}^{\mathrm{BAE}}[\omega] = \bar{S}_{\mathrm{meas}}^{\mathrm{BAE}}[\omega] - \bar{S}_0[\omega] = \bar{S}_c[\omega] + \bar{S}_{\mathrm{BAE}}[\omega], \tag{30}$$

the first term $\bar{S}_c[\omega]$ is the noise spectrum of the cavity resonance due to the non-zero cavity occupation. The second term $\bar{S}_{\mathrm{BAE}}[\omega]$ is the noise spectrum of the BAE sideband, which is given by

$$\bar{S}_{\mathrm{BAE}}[\omega] = \mathcal{G}[\omega_c]\,\kappa_R \hbar\omega_c \frac{4g_0^2}{\kappa} n_p \frac{\kappa}{\kappa^2 + 4\Delta^2} \frac{S_{X_\phi}[\omega]}{x_{zp}^2}, \tag{31}$$

where $S_{X_\phi}[\omega]$ is the mechanical quadrature spectrum. Because the BAE sideband is detuned from the cavity resonance with detuning comparable to the cavity linewidth, over the bandwidth of the BAE measurement, the cavity noise appears as a frequency dependent noise background. An example of the spectrum is given by Fig. S6, a quadratic polynomial is employed to fit the cavity noise background, as shown by the red curve in Fig. S6. The BAE sideband spectrum $\bar{S}_{\mathrm{BAE}}[\omega]$ is given by subtracting the noise spectrum from the fitted cavity noise background. The noise power of the BAE sideband is given by integrating Eq. (31), which gives

$$P_m^{\mathrm{BAE}} = \mathcal{G}[\omega_c]\,\kappa_R \hbar\omega_c n_p \frac{4g_0^2}{\kappa^2 + 4\Delta^2} \frac{\left\langle X_\phi^2 \right\rangle}{x_{zp}^2}. \tag{32}$$

With the thermal calibtration factor b_-^{BAE}, we can convert the normalized BAE sideband power to the quadrature variance

$$\frac{\left\langle X_\phi^2 \right\rangle}{x_{zp}^2} = \frac{1}{b_-^{\mathrm{BAE}}} \left(\frac{4\Delta^2 + \kappa^2}{4} \right) \frac{P_m^{\mathrm{BAE}}}{P_-}. \tag{33}$$

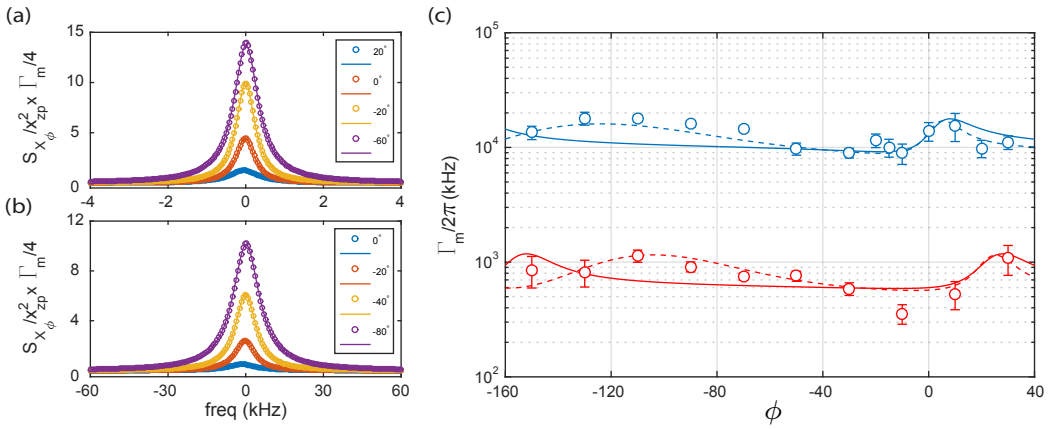

FIG. S7. The predicted mechanical quadrature spectra calculated with Eq. (19) (circles) and the corresponding Lorentzian fits (solid curves). (a) The predicted mechanical quadrature spectra and Lorentzian fits correspond to the dashed red curve in Fig. 2c in the main text. (b) The predicted mechanical quadrature spectra and Lorentzian fits correspond to the dashed blue curve in Fig. 2c in the main text. (c) Quadrature linewidth as a function of the probe phase. The red (blue) circles are the measured quadrature linewidth of the weakly (strong) squeezed state using the BAE technique. The curves are the fits with the two-tone optomechanical model including the mechanical parametric effect. The solid curves are the fits with the assumption $\psi = \psi_0$. The dashed curves are the fits with the assumption $\psi = \phi + \psi_0$.

IV. ANALYSIS OF THE MECHANICAL PARAMETRIC EFFECT

In this section, we will describe the procedures to extract the mechanical parametric interaction from the measured quadrature linewidth data. As shown in the theory section, for given pump configurations $(\Delta, \delta, n_p^{\pm})$, thermal occupations $(n_m^{\rm th}, n_c^{\rm th})$ and mechanical parametric interaction (λ, ψ), the mechanical quadrature spectrum $\bar{S}_{X_\phi}[\omega]$ can be calculated by Eq. (19). The mechanical quadrature linewidth is given by fitting the predicted mechanical quadrature spectrum with a Lorentzian curve, as shown in Fig. S7a(b).

Using the pump configurations and thermal occupations extracted from the corresponding output spectra (Fig. 1f,g in the main text), the quadrature linewidth can be written as a function of the probe phase ϕ, the amplitude λ and the phase ψ of the parametric drive (i.e. $\Gamma_m^{\rm p}(\phi, \lambda, \psi)$). Then we can extract the mechanical parametric interaction (λ, ψ) by fitting the measured mechanical quadrature linewidth in the BAE measurement with the function $\Gamma_m^{\rm p}(\phi, \lambda, \psi)$.

As discussed in the main text, we assume the phase of the parametric drive ψ follows the phase of the BAE probe ϕ (i.e. $\psi = \psi_0 + \phi$, where ψ_0 is a constant phase shift). The amplitude λ and the constant phase shift ψ_0 can be extracted by fitting the quadrature linewidth data with the function $\Gamma_m^{\rm p}(\phi, \lambda, \psi_0 + \phi)$, the fit results are shown by the dashed curves in Fig. S7c. From the fit, we extract $\lambda = 2\pi \times (121 \pm 34)$Hz, $\psi_0 = -121^\circ \pm 52^\circ$ for the weakly squeezed state (red dashed curve) and $\lambda = 2\pi \times (1.3 \pm 0.3)$kHz, $\psi_0 = -129^\circ \pm 15^\circ$ for the strong squeezed state (blue dashed curve). Under this assumption, the model captures the observed phase dependence behavior of the quadrature linewidth in the BAE measurement. With the extracted mechanical parametric drive, the corresponding quadrature variances can be calculated by Eq. (20), as shown by the dashed curves in Fig. 2b in the main text. On the other hand, if we assume the mechanical parametric drive is induced by the squeezing pump (i.e. $\psi = \psi_0$), the function $\Gamma_m^{\rm p}(\phi, \lambda, \psi_0)$ doesn't capture the observed phase dependence behavior of the mechanical quadrature linewidth, as shown by the solid curves in Fig. S7c. These results imply that the observed mechanical parametric interaction is induced by the BAE probes instead of the squeezing pumps.

V. ENGINEER AND OPTIMIZE THE MECHANICAL PARAMETRIC DRIVE

Having established a phenomenological model to understand the effects of the mechanical parametric drive to the squeezed states obtained from the reservoir engineering technique, the next step is to engineer and optimize it to further increase the squeezing. As described in the main text the parametric drive in our experiment is induced by the uncontrollable nonlinear processes [1]. Therefore, the amplitude and phase of the parametric drive cannot be controlled independently in the current experiment. In order to implement a tunable mechanical parametric drive, one can add an additional electrode to drive the mechanical oscillator [4, 5]. By applying an ac drive $V(t) = V_0 + V_p \sin(2\omega_m t + \psi_0)$ to the electrode, it generates a time varying spring constant $k_p(t) = \Delta k \sin(2\omega_m t + \psi_0)$ with $\Delta k = \left(\partial^2 C/\partial x^2\right) V_0 V_p$.

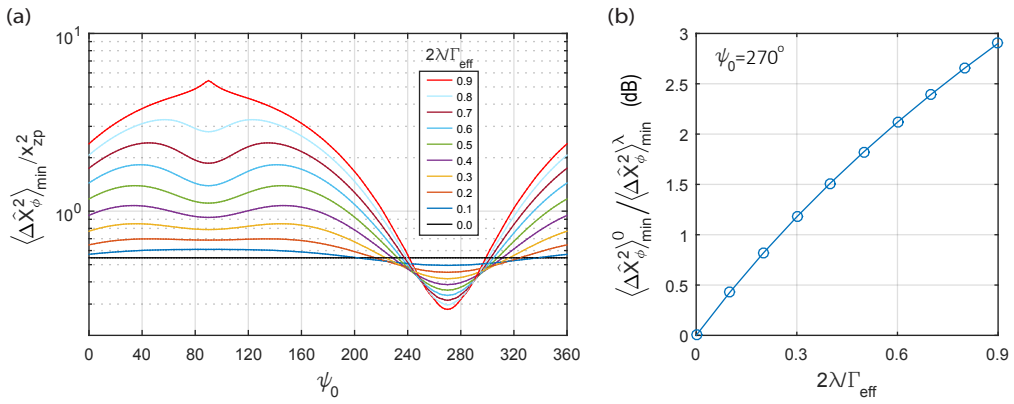

FIG. S8. (a) Minimum quadrature variance as a function of phase ψ_0. Different curves represent different parametric drive amplitude λ. (b) The Minimum quadrature variance at the optimum phase ($\psi_0 = 270°$) as a function of the parametric drive amplitude λ.

This in turn yields the tunable mechanical parametric interaction

$$\hat{H}_{\rm para} = \hbar\lambda(e^{i\psi_0}\hat{b}^2 + e^{-i\psi_0}\hat{b}^{\dagger 2}), \tag{34}$$

where $\lambda = \Delta k x_{\rm zp}^2/4\hbar$. The amplitude and phase of the parametric drive can be controlled by the gate voltage V_0 and the phase of the ac drive ψ_0. The uncontrollable mechanical parametric drive induced by the BAE probe can be diminished by reducing the power of the BAE probes.

Given the linearity of the mechanical dynamics, the mechanical parametric drive in Eq. (34) could be used to directly augment the squeezing generated optomechanically. One simple chooses the phase ψ_0 such that the parametric drive preferentially damps the squeezed X_1 mechanical quadrature. As one approaches the parametric instability, the damping rate of this quadrature is doubled, leading to an additional 3dB of squeezing beyond what would be achieved just via the optomechanical scheme.

To illustrate this, we show below explicit theoretical results including both the parametric drive and optomechanical interaction. Fig. S8a shows the minimum mechanical quadrature variance at different phase ψ_0 and amplitude λ. In this plot, we use the same squeezing pump configuration and thermal occupations in Fig. 1g in the main text. As shown in the figure, the minimum mechanical quadrature variance is very sensitive to the phase. The additional mechanical parametric effect can worsen or improve the squeezing depending on the phase. The black line is the result with the reservoir engineering squeezing alone ($\lambda = 0$). At the optimum phase ($\psi_0 = 270°$), the amount of squeezing increases with the parametric drive amplitude (Fig. S8b). The parametric drive amplitude is limited to $\lambda = \Gamma_{\rm eff}/2$ due to the onset of the parametric instability, which place a fundamental limit to the additional squeezing. As shown in Fig. S8b, the mechanical parametric drive can provide additional 3 dB squeezing to the squeezed state generated by the reservoir engineering scheme.

[1] J. Suh, A. J. Weinstein, and K. C. Schwab, Appl. Phys. Lett. **103** (2013).
[2] J. Suh, M. D. Shaw, H. G. LeDuc, A. J. Weinstein, and K. C. Schwab, Nano Lett. **12**, 6260 (2012).
[3] A. J. Weinstein, C. U. Lei, E. E. Wollman, J. Suh, A. Metelmann, A. A. Clerk, and K. C. Schwab, Phys. Rev. X **4**, 041003 (2014).
[4] D. Rugar and P. Grütter, Phys. Rev. Lett. **67**, 699 (1991).
[5] R. Andrews, A. Reed, K. Cicak, J. Teufel, and K. Lehnert, Nat. Commun. **6**, 10021 (2015).